Journal of Chromatography A, xxx (2018) xxx–xxx

Contents lists available at ScienceDirect

Journal of Chromatography A

journal homepage: www.elsevier.com/locate/chroma

Design keys for paper-based concentration gradient generators

Federico Schaumburg[a], Raúl Urteaga[b], Pablo A. Kler[c,d,*], Claudio L.A. Berli[a,**]

[a] Instituto de Desarrollo Tecnológico para la Industria Química (INTEC, UNL–CONICET), Colectora RN 168 Km 472, S3000GLN Santa Fe, Argentina
[b] Instituto de Física del Litoral (IFIS Litoral, UNL–CONICET), Güemes 3450, S3000GLN Santa Fe, Argentina
[c] Centro de Investigación de Métodos Computacionales (CIMEC, UNL–CONICET), Colectora RN 168 Km 472, S3000GLN Santa Fe, Argentina
[d] Departamento de Ingeniería en Sistemas de Información, FRSF-UTN, Lavaise 610, S3004EWB Santa Fe, Argentina

ARTICLE INFO

Article history:
Received 4 March 2018
Received in revised form 15 May 2018
Accepted 20 May 2018
Available online xxx

Keywords:
Mechanical dispersion
Paper based microfluidics
Paper based gradient generators
Solute transport

ABSTRACT

The generation of concentration gradients is an essential operation for several analytical processes implemented on microfluidic paper-based analytical devices. The dynamic gradient formation is based on the transverse dispersion of chemical species across co-flowing streams. In paper channels, this transverse flux of molecules is dominated by mechanical dispersion, which is substantially different than molecular diffusion, which is the mechanism acting in conventional microchannels. Therefore, the design of gradient generators on paper requires strategies different from those used in traditional microfluidics. This work considers the foundations of transverse dispersion in porous substrates to investigate the optimal design of microfluidic paper-based concentration gradient generators (μPGGs) by computer simulations. A set of novel and versatile μPGGs were designed in the format of numerical prototypes, and virtual experiments were run to explore the ranges of operation and the overall performance of such devices. Then physical prototypes were fabricated and experimentally tested in our lab. Finally, some basic rules for the design of optimized μPGGs are proposed. Apart from improving the efficiency of mixers, diluters and μPGGs, the results of this investigation are relevant to attain highly controlled concentration fields on paper-based devices.

1. Introduction

Microfluidic paper-based analytical devices (μPADs) is nowadays a well established technology, as demonstrated in different topical review papers [1–4]. Nevertheless, several aspects related to transport of species in the porous substrate are still to be improved to reach higher levels of efficiency. For example, the amount of analyte effectively transported by the flow and the details of sample distribution in complex geometries are central issues for analytical operations implemented on μPADs [5]. In particular, the generation of concentration gradients is a key operation in microfluidic platforms for drug discovery, bacterial growth, cell culture, and chemotaxis studies [6]. Actually, several of these procedures are being implemented on μPADs [7–10]. However, scientific reports on the generation of concentration gradients on paper are still a few: the conventional tree-like network [11], co-flow in Y-shaped channel [12], and multiple co-flows in a wide single channel [13], to the best of our knowledge. Closely related works are those dealing with mixing operations [14,15], where the transverse dispersion of species is also involved. In this context, the design of effective and versatile microfluidic paper-based gradient generators (μPGGs) deserves further investigation, and this is precisely the goal of the present work.

A central aspect here is that solute dispersion in porous media is mostly due to mechanical dispersion, a mechanism inherent to the random character of the pore network [16]. Although this effect is well documented in the literature related to transport in porous media [17,18], the subject has not been considered in the field of paper-based microfluidics until a topical work [19], where we have discussed the physical basis of transverse solute dispersion in filter paper by theory and experiments. The outcome of this study is essential for the accurate design of operations requiring precise spatial distribution of analytes or reactants, notably the generation of concentration gradients. To put this knowledge in perspective, it is worth to briefly review the conventional methods.

Microfluidics gradient generators fabricated with conventional microchannels may be divided in two main categories: statics and dynamics. In the first case, the concentration gradient is gener-

* Corresponding author at: Centro de Investigación de Métodos Computacionales (CIMEC, UNL–CONICET), Colectora RN 168 Km 472, S3000GLN Santa Fe, Argentina.
** Corresponding author at: Instituto de Desarrollo Tecnológico para la Industria Química (INTEC, UNL–CONICET)., Colectora RN 168 Km 472, S3000GLN Santa Fe, Argentina.
E-mail addresses: kler@cimec.unl.edu.ar (P.A. Kler), cberli@santafe-conicet.gov.ar (C.L.A. Berli).

https://doi.org/10.1016/j.chroma.2018.05.040
0021-9673/

ated in a chamber with stagnant flow, which is constantly feed with fresh reactants from opposite side ports, so that controlled diffusion-based gradients are achieved, including sophisticated spatio-temporal distributions [20–22]. Dynamic generators also rely on molecular diffusion, though in this case the species diffuse across parallel flow streams with different initial concentrations, thus a concentration gradient orthogonal to the flow is formed at a certain downstream distance [23,24]. Further, this transverse mixing taking place after T- or Y-shaped junctures is the elementary process used to generate gradients at larger scales by using microchannel networks, such as the tree format for linear gradients [25,26], or asymmetric configurations for non-linear gradients [27,28] and serial dilutions [29,30].

In the gradient generators mentioned above, a balance between diffusive and advective transports has to be found to optimize mixing performance. Thus, the design is constrained by the molecular diffusivity of species, the desired flow rate, and microchannel length. In contrast, the underlying mechanism of transverse dispersion in paper is substantially different, since it is dominated by mechanical dispersion in the pore space. More precisely, the gradient formation is independent on fluid velocity and fully determined by the paper microstructure [19]. This information reveals that the design of μPGGs requires strategies different from those used for conventional microchannels. Indeed, a change of paradigm is envisioned for the rationalization of gradient generators in paper-based devices [13]. The present work investigates the problem by numerical simulations based on the appropriate theory for species transport in porous media. A set of novel, versatile, and easy-to-build μPGGs were designed in the form of numerical prototypes. After running virtual experiments, physical prototypes were constructed and tested to prove the concepts. Finally, some basic rules to be considered for the design of effective and optimized μPGGs are proposed.

2. Numerical simulations

2.1. Theoretical background

This section briefly discusses the physical basis of the model and the main equations used to solve the transport of species in paper substrates. Firstly, the capillary-driven fluid dynamics is solved by using an effective medium approach, as recently reported for nitrocellulose and similar porous substrates [31]; further explanations are given next in Section 2.2. A macroscopic velocity field **u** is obtained, which is defined by fluid viscosity, porosity, permeability, and the geometrical boundaries of the fluid domain. Coupled to this velocity field, the macroscopic species concentration field (that already considers the local porosity) C is governed by the following equation:

$$\frac{\partial C}{\partial t} = \nabla \cdot \mathbf{J} \tag{1}$$

where the **J** is the total mass flux for the species. For weakly concentrated species in the porous matrix, **J** is introduced as the linear superposition of advective, diffusive and mechanical-dispersive transport mechanisms, respectively [32,33],

$$\mathbf{J} = \mathbf{u}C - D_0 \nabla C - s|\mathbf{u}|\nabla C \tag{2}$$

where D_0 is the molecular diffusion coefficient and s is the dispersivity constant, which represents a characteristic dimension of the fiber network microstructure. The last term in Eq. (2) is characteristic of porous media, where the alternating variation of pore-level fluid velocity, in both magnitude and direction, produces a mechanical dispersion. This mechanism is normally characterized by a mechanical dispersion coefficient D_m, which can be differentiated in the longitudinal, $D_{m,L} = s_L u_L$, and transverse $D_{m,T} = s_T u_L$, directions [16–18]. In these expressions, s_L and s_T are the dispersivities in the longitudinal and transverse directions, respectively, and u_L is the average fluid velocity in the longitudinal direction of the flow. It is known that s_L is larger than s_T, however, as this work is focused on μPGGs, where the solute dispersion transverse to the flow is the main concern for the design, the isotropic formulation $s|\mathbf{u}|\nabla C$ is considered to be adequate, and hereafter we use $s = s_T$. This coefficient was measured to be $s = 30\ \mu m$ for the transverse dispersion of solutes in Whatman grade 1 filter paper [19]. It is worth noting that, for the typical fluid velocities developed in paper-based microfluidics, $s|\mathbf{u}| \gg D_0$, thus transverse solute dispersion is predominantly driven by the mechanical process. Molecular diffusion contributes to the total dispersion when fluid velocity decreases up to the critical value $|\mathbf{u}|_c = D_0/s$. Of course, if $|\mathbf{u}| \to 0$, there is no advection in the pore space, and molecular diffusion is the only active mechanism.

In order to gain more insight on the problem, following we introduce an analytical solution of Eq. (1) for steady 1D flows, which was already studied in [19] and will be also used next for model validation. The flow domain for this basic problem is schematically shown in Fig. 1a: it represents a porous substrate with co-flowing streams of average velocity u_y, one of them transporting a given species of initial concentration C_0. For constant u_y, this problem is equivalent to that with stagnant flow and molecular diffusion in the x-direction, considering that the time-evolution of $C(x, t)$ is observed at each transect $y = u_y t$ along the flow path. Then the concentration profile $C(x, y)$ is governed by,

$$u_y \left(\frac{\partial C}{\partial y} \right) = D \left(\frac{\partial^2 C}{\partial x^2} \right) \tag{3}$$

which derives form Eq. (1) via the change of variable $t = y/u_y$ and a generic coefficient D that condenses diffusive and dispersive effects. Besides, in flow conditions where molecular diffusion is negligible compared to mechanical dispersion, the coefficient can be included directly as $D = su_y$, and the governing equation results,

$$\frac{\partial C}{\partial y} = s \left(\frac{\partial^2 C}{\partial x^2} \right). \tag{4}$$

Given the boundary conditions $[C(x \to -\infty) = C_0,\ C(x \to \infty) = 0]$ for the problem stated, the solution of Eq. (4) is [34],

$$\frac{C(x, y)}{C_0} = \frac{1}{2} erfc \left[\frac{x}{2(sy)^{1/2}} \right] \tag{5}$$

It is worth noting that the concentration field predicted by Eq. (5) becomes independent of the fluid velocity field. Therefore, three relevant corollaries emerge from Eq. (5): (i) the dispersion width $\sigma_x = (sy)^{1/2}$ is independent of fluid velocity and species characteristics, (ii) the gradient formation is fully determined by the dispersivity s (paper microstructure), and (iii) the transverse solute dispersion is several times larger than the one expected for molecular diffusion.

Concerning the range of validity of this modeling, it should be mentioned that for capillary-driven flows in uniform strips, $u_y = c/y$, where c is the dynamic coefficient that characterizes each paper substrate [35]. Thus the hypothesis of dominant mechanical dispersion is satisfied at distances shorter than $y_c = cs/D_0$. For aqueous solutions in Whatman 1 paper, this critical distance is around 1 m, which means that Eqs. (4 and 5) are fairly valid in paper-based microfluidics. The flow regimes can be also characterized by the Peclet number, which is defined at the pore level as $Pe = su_y/D_0$ [16,17]. In this context, mechanical dispersion prevails over diffusion when $Pe \gg 1$, which is largely the case for Whatman 1 filter paper [19]. These concepts will be used along this work to generate the design rules for μPPGs summarized in the conclusions.

Please cite this article in press as: F. Schaumburg, et al., Design keys for paper-based concentration gradient generators, J. Chromatogr. A (2018), https://doi.org/10.1016/j.chroma.2018.05.040

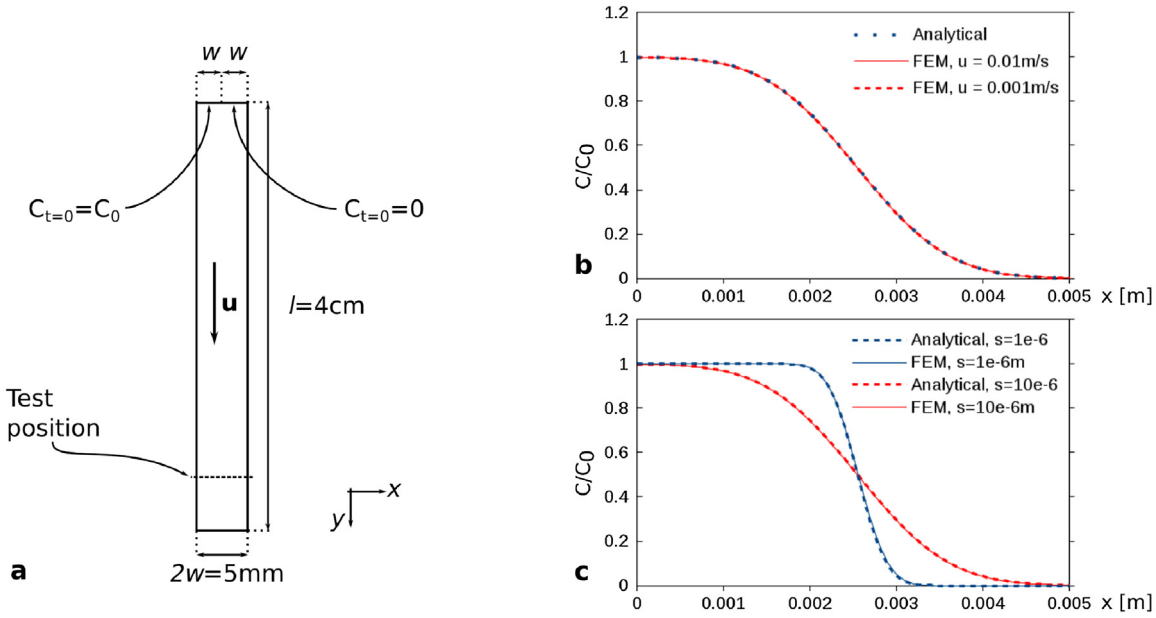

Fig. 1. Numerical model validation. (a) Problem statement: paper strip dimensions, initial concentration, and fluid velocity direction. (b) Relative concentration as a function of transverse distance, at the test position $y = 3.5$ cm indicated in Fig. 1a. Curves are the analytical solution (Eq. (5)) and numerical prediction for $u_y = 0.01$ ms^{-1} and $u_y = 0.001$ ms^{-1}. (c) Idem in (b) for $s = 1$ μm and $s = 10$ μm.

2.2. Methodology

Fluid dynamic and mass transfer problems in the porous matrix are described by continuum transport equations. The model involves volume-averaged variables by using the concept of elementary representative volume (see, for example, [36]). More precisely, the fluid velocity is computed on a characteristic length that is defined on an intermediate scale, much larger than the pore size, but smaller than the analysis domain considered, avoiding to describe the local flow through the intricate pore space. It is relevant to note that the mechanical dispersion, which intrinsically depends on splitting and combinations at the pore level, is also computed here as a macroscopic effect expressed in terms of the averaged fluid velocity (Eq. (2)).

The flow is also assumed to be pseudo-stationary and free of inertia, in agreement with the extremely low local Reynolds numbers. The system is considered to be under isothermal conditions and with controlled humidity level. Gravity is ignored in the analysis taking into account that the Bond number is negligible. With these assumptions, mass conservation equation for incompressible fluids can be coupled to Darcy's law [35],

$$\begin{aligned} \nabla\cdot(\phi\mathbf{u}) &= 0 \\ \mathbf{u} &= -\frac{\kappa}{\mu\phi}\nabla p \end{aligned} \tag{6}$$

where κ is the paper permeability, μ is the fluid viscosity, ϕ the porosity and ∇p is the pressure gradient. These expressions can be combined and used for calculating the pressure field,

$$\begin{aligned} \nabla\cdot(\kappa\nabla p) &= 0 \\ p &= 0 \quad \text{at} \quad \Gamma_s \end{aligned} \tag{7}$$

$$\begin{aligned} p &= p_{Lap} \quad \text{at} \quad \Gamma_f \\ \nabla p\cdot\mathbf{n} &= 0 \quad \text{at} \quad \Gamma_{Wall} \end{aligned} \tag{8}$$

Eqs. (7) and (8) are the boundary conditions at the fluid source and front, respectively. In the problems solved in this work, Γ_s coincides with fluid inlets where (for simplicity) the pressure can be fixed to zero, and Γ_f coincides with fluid outlets, where p_{Lap} is the Laplace capillary pressure [31]. Also, $\mathbf{n}$ is a vector normal to the Γ_{Wall} boundaries. Once the p is calculated, velocity field can be obtained directly from Eq. (6), where $\kappa = 7.5\times10^{-16}$ m^2 and $\phi = 0.68$ were used. Then the concentration field is calculated by combining Eqs. (1 and 2), which gives the following boundary value problem,

$$\begin{aligned} \frac{\partial C}{\partial t} &= \nabla\cdot(\mathbf{u}C - D_0\nabla C - s|\mathbf{u}|\nabla C) \\ C &= C_0 \quad \text{at} \quad \Gamma_{inlet} \\ \nabla C\cdot\mathbf{n} &= 0 \quad \text{at} \quad \Gamma_{outlet} \quad \text{and} \quad \Gamma_{wall} \end{aligned}$$

where C_0 is a concentration distribution. In all calculations, $C_0 = 40\times10^{-6}$M and $D_0 = 6.5\times10^{-10}$ m^2 s^{-1} were considered.

The simulation scheme involves the iterative calculations for the coupled fields of pressure, fluid velocity, and species concentration. A detailed description of this numerical tool and coefficients and parameter values representing fluid properties can be found elsewhere [31]. A novel contribution here is the computation of the mass flux from Eq. (2), which involves additional coupling between the velocity and concentration fields related to the mechanical dispersion.

Computer simulations were performed with the *Finite Element Method* by using the program PETSc–FEM [37] in a Python environment. Mesh details are summarized in Table S1 in the supplementary material, for each particular case. Also in the supplementary material, Section S1 shows that results are independent of mesh density. For the solution of fluid flow, the *Conjugate Gradient* method preconditioned with *Boomer* algebraic multigrid algorithm was used. Regarding transport equation solution, the *Generalized Minimal Residual* method was used with an *Additive Schwarz* decomposition algorithm with five layer overlapping with incomplete LU preconditioning. In both cases, nonlinear convergence tolerance was set to 10^{-9}. The hardware employed was a desktop computer with a single quad-core Intel i7 7700 3.6 GHz processor and 16 GB DDR3–2400 memory. In every case, 4 calculation threads were used.

Please cite this article in press as: F. Schaumburg, et al., Design keys for paper-based concentration gradient generators, J. Chromatogr. A (2018), https://doi.org/10.1016/j.chroma.2018.05.040

2.3. Validation

Computer simulations were verified against the prediction of Eq. (5) for 1D flow domains. It is relevant to point out that this analytical solution had been validated against experiments in our previous work [19]. Therefore, crosschecking the simulations with the analytical solution also constitutes a validation of the numerical model. Effectively, the computer simulations were compared to the prediction of Eq. (5) for the straightforward system schematized in Fig. 1a. The following boundary conditions were used: $[C(-w \le x \le 0, y = 0) = C_0, C(0 < x \le w, y = 0) = 0, \frac{\partial C}{\partial x}(x = -w) = 0, \frac{\partial C}{\partial x}(x = w) = 0]$. The results are plotted in Fig. 1b–c, together with the prediction of Eq. (5). In Fig. 1b, different values of u_y were used to check if numerical solutions predict a dispersion width independent of fluid velocity. In Fig. 1c, different values of s were used to analyze the response of the model to this parameter. In all cases, the numerical model satisfactorily predicts the expected behavior. These calculations also serve as the starting point for discussions in Section 3.

3. Gradient generation: the elementary process

The 1D problem discussed above is the simplest way to form concentration gradients in paper. Here, a 2D domain is considered in order to include the inlet ports for the fluids. A standard Y-shaped juncture was chosen for calculations, as shown in Fig. 2a. Fig. 2b presents the predicted concentration profiles, where curves correspond to transects at different downstream distances (indicated in Fig. 2a). It is observed that the step-like function formed immediately after the Y-juncture evolves into a less slanted and more linear profile along the flow path, and reaches a flat profile for sufficiently long channels. This limit is useful for mixers, as perfect mixing of interdiffusing species can be achieved, however it is pernicious for the formation of a concentration gradient, as the dynamic range (DR) is minimum, being $DR = C_{MAX} - C_{MIN}$, where C_{MAX} and C_{MIN} are the maximum and minimum concentration values respectively. Thus, a trade-off between linearity and DR must be reached. In Fig. 2a, for example at $y = 1$mm, the concentration gradient is fairly linear and DR is about $0.75C_0$.

Here, the channel width deserves special considerations. The argument of $erfc$ function in Eq. (5), $\gamma = x/(2(sy)^{1/2})$, defines the desired species concentration at a downstream position x, y. Therefore, the strip length ($y = l$) required to attain a gradient expanding the channel width ($x = w$) obeys to:

$$l = \frac{w^2}{4\gamma^2 s} \tag{9}$$

It is evident from Eq. (9) that, by decreasing w, the desired gradient can be formed in a shorter channel. This is a consequence of the fact that the dispersion width $\sigma_x = (sy)^{1/2}$ is independent of fluid velocity. And the overall result is that the gradient formation is much more efficient in paper-based devices than in conventional microchannels: the mechanical dispersion forms the gradient in relatively short distances, given the same channel width and flow rate. Furthermore, the length of a conventional open microchannel has to be su_y/D_0 times larger than the paper channel to attain the same solute dispersion (see [19] for further details).

4. Gradient amplification

4.1. Straight outlet

It was demonstrated above that a concentration gradient can be readily formed in a single channel. The gradient can be naturally linear with the desired DR. It was also shown that the channel needs to be thin, in order to achieve the required gradient in a downstream distance as short as possible, hence decreasing the overall size of the device. Nevertheless, the drawback of small width channels is that the outlet may become unpractical to supply the generated gradient to subsequent chemical or biological operations. An interesting proposal to circumvent this problem has been reported in a recent work [13], where multiple inlets with different concentrations were used to attain a wider channel with uniform section. As an advantageous alternative, here we propose to amplify the gradient formed in the Y-shaped channel simply by opening the flow domain as a diffuser. In this section we discuss how the spatial range of the gradient can be expanded while maintaining the concentration profile.

The first aspect to consider is the geometrical constraint required to maintain the formed concentration gradient, being the opening angle the most important variable to assess. For example, if a 1 cm wide outlet is required, the original gradient width (1 mm) needs a 10 times amplification, and the channel length will be a function of the opening angle. This is shown in Fig. 3a where the resulting analyte concentration profiles are shown for four devices with angles ranging from 10° to 45°. In particular the concentration at each outlet is plotted in Fig. 3b, where it can be seen how DR increases with the opening angle. This is because, for the same outlet width, the traveled distance is shorter for larger angles. The DR obtained for each device at different distances from the expansion onset are shown in Fig. 3c. It is observed that DR decreases with downstream distance (due to mechanical dispersion) and the curves reach an asymptotic behavior after a certain distance. To explain this, it should be recalled that $s = \sigma_x^2/\Delta y$, where σ_x is the dispersion width in the x-direction when the fluid travels a distance Δy in the y-direction [19]. Besides, the expansion angle is $\alpha = \arctan(\Delta x/\Delta y)$ where Δx is the maximum distance covered in the x-direction due to the geometrical expansion in the diffuser. Then, if an equilibrium between dispersion and expansion is considered, i.e. $\sigma_x = \Delta x$, for a small value of α, the following relation is obtained,

$$\Delta y_c = \frac{s}{tg^2\alpha} \tag{10}$$

where the subindex c indicates that Δy_c is a critical distance. When $\Delta y \ll \Delta y_c$ the mechanical dispersion generates a DR loss in the concentration distribution. In contrast, when $\Delta y \gg \Delta y_c$ the dispersion width is shorter than the separation among streamlines in the x-direction caused by the expansion of the flow domain, which leads to constant concentration in the device borders for any Δy. This last situation suggests the possibility to *cool-down* the concentration profile. According to Eq. (9), if $\alpha = 0°$ (such as in Fig. 2), then $\Delta y_c \to \infty$, meaning that the cooling-down effect is never reached. If $\alpha = 45°$ then $\Delta y_c = s$, and the DR is preserved, since the critical distance is on the order of s, which spans in the micrometer scale [19].

The second aspect to consider is the variation of the fluid front profile after the expansion. In fact, mass conservation transforms its initially straight profile into an elliptical one, as observed in Fig. 4a, for an arbitrary angle. Nevertheless, Fig. 4b shows that the concentration profile taken over the elliptical front practically coincides with those taken over straight transects at similar distances. Actually, once that Δy_c is reached, the concentrations in the diffuser borders assume constant values (C_{MAX} and C_{MIN} respectively) and thus, as the C-field is continuous, practically any concentration profile in the $[C_{MIN}, C_{MAX}]$ range can be obtained if the proper cut line is found. As an example, the bilinear black-dotted cut line in Fig. 4a produces a linear-like concentration, as plotted in Fig. 4b. This result suggests that different geometrical shapes can be used at the outlet. This information is relevant for design purposes and will be exploited next in Section 4.2.

Please cite this article in press as: F. Schaumburg, et al., Design keys for paper-based concentration gradient generators, J. Chromatogr. A (2018), https://doi.org/10.1016/j.chroma.2018.05.040

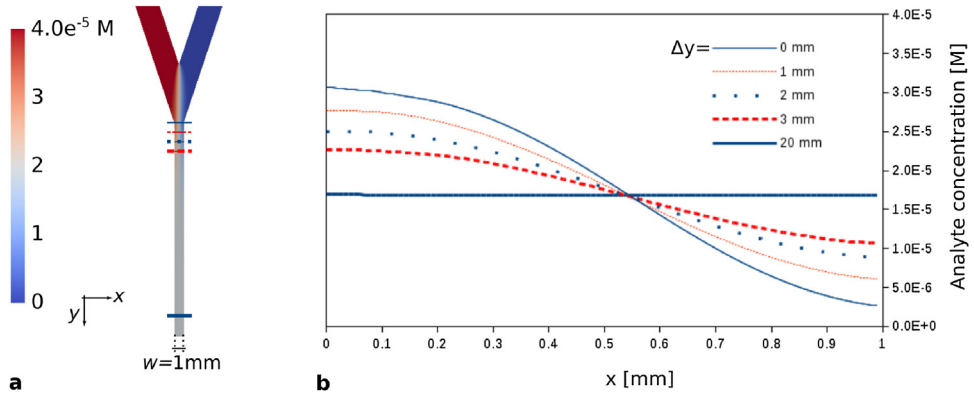

Fig. 2. Concentration gradient profiles in a paper strip. (a) Concentration profiles of co-flowing streams in a Y-shaped paper-based device with $|u| = 0.0002\,\mathrm{ms}^{-1}$. (b) Concentration as a function of transverse distance at different positions Δy along the flow path.

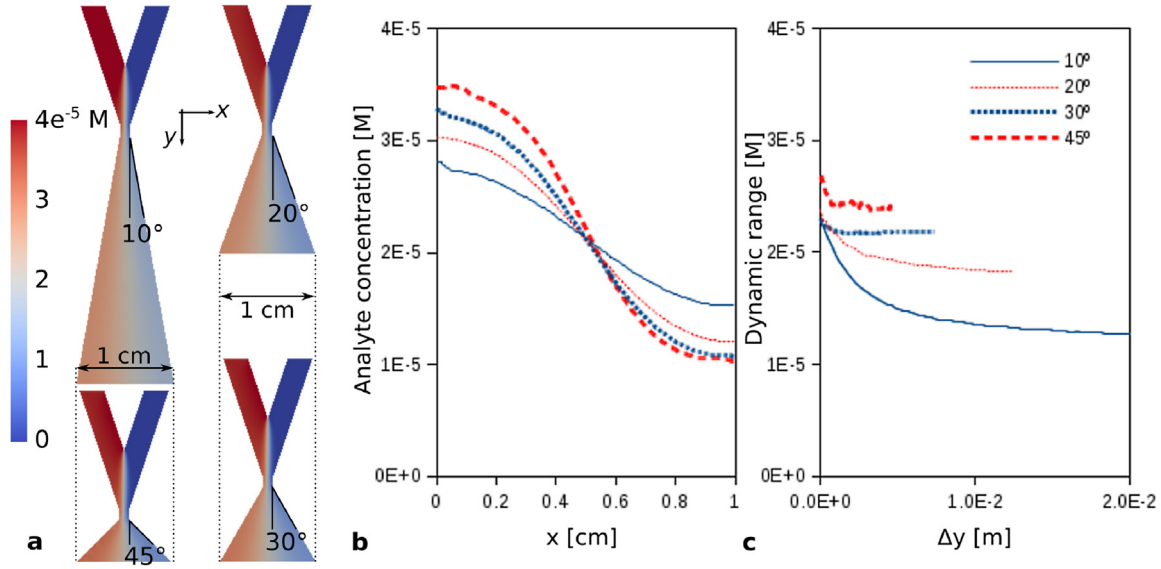

Fig. 3. Amplification of concentration gradients: opening angles. (a) Concentration profiles obtained in diffusers with angles between 10 and 45°. (b) Concentration as a function of transverse distance at the outlet of each diffuser. (c) *DR* as a function of the downstream distance for each diffuser.

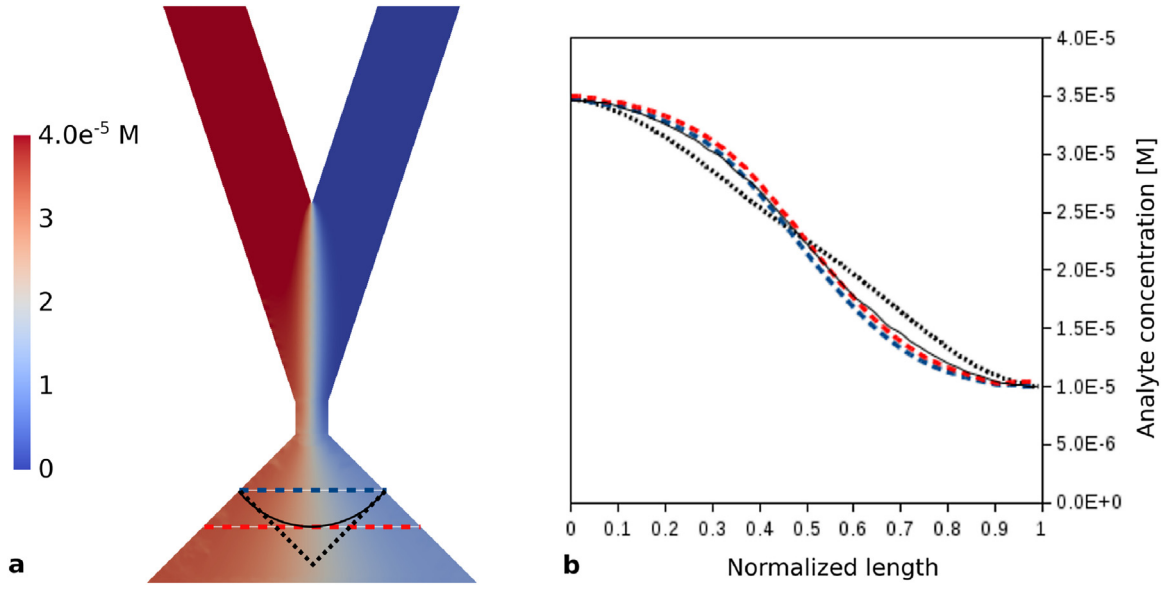

Fig. 4. Amplification of concentration gradients: outlet contours. (a) Different cut lines considered in the diffuser. (b) Concentration as a function of transverse distance on different cut lines, the contour lengths of which were self-normalized for better comparison.

Please cite this article in press as: F. Schaumburg, et al., Design keys for paper-based concentration gradient generators, J. Chromatogr. A (2018), https://doi.org/10.1016/j.chroma.2018.05.040

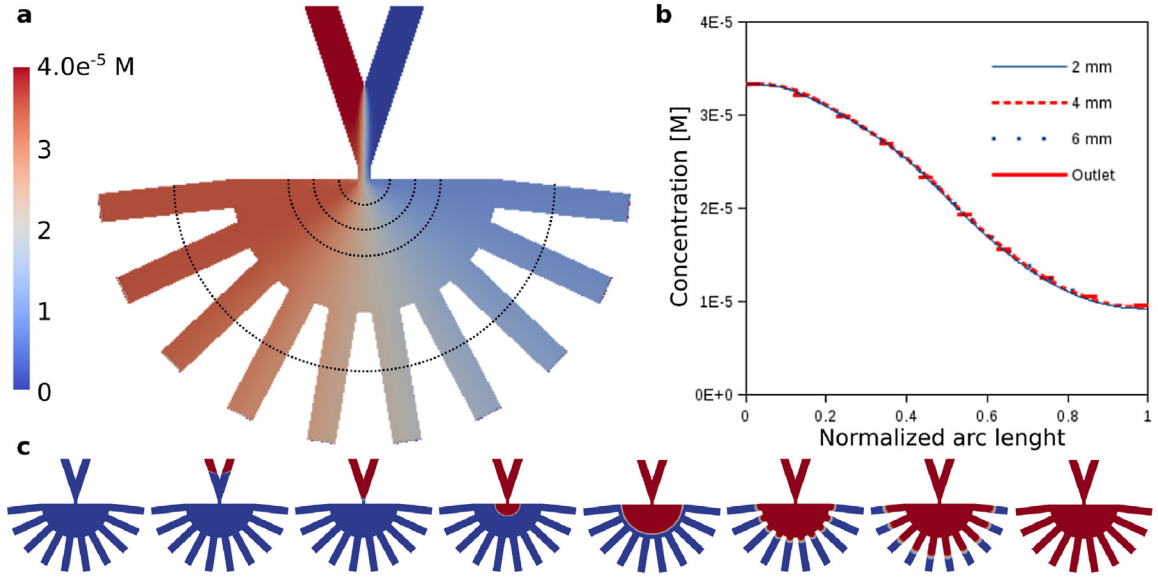

Fig. 5. Ellipsoidal outlet gradient generator. (a) Concentration distribution obtained by numerical simulations. (b) Concentration as a function of the transverse distance along the ellipsis defined in a). (c) Different time steps during the filling process of the paper device, where the red claret color denotes the instantaneous fluid front. (For interpretation of the references to color in this figure legend, the reader is referred to the web version of this article.)

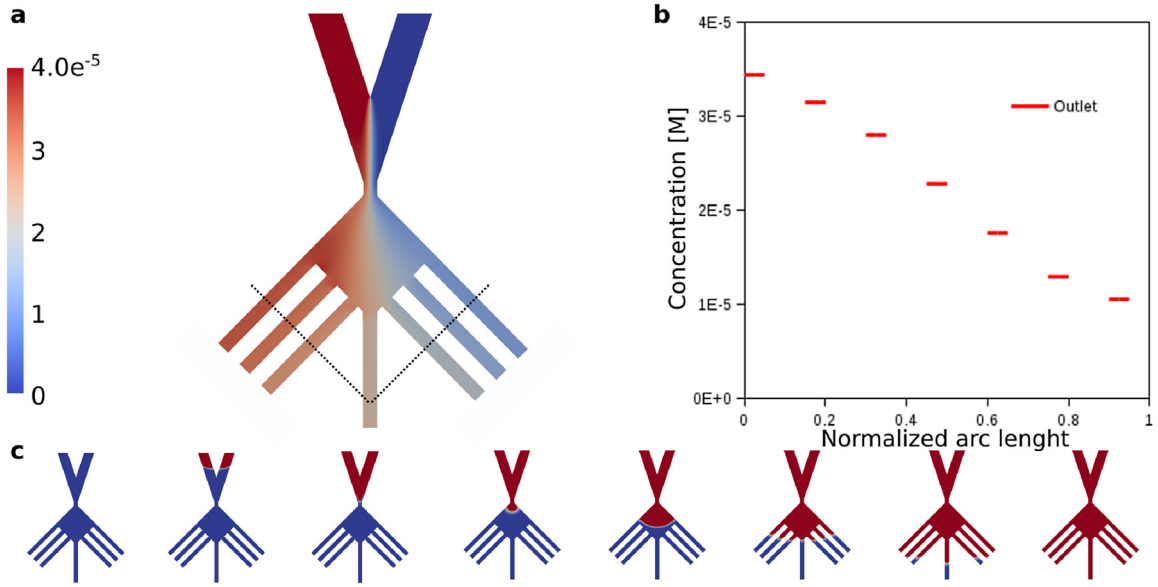

Fig. 6. Bilinear outlet gradient generator. (a) Concentration distribution obtained by numerical simulations. (b) Average concentration in the discrete outlets. (c) Different time steps during the filling process of the paper device, where the red claret color denotes the instantaneous fluid front. (For interpretation of the references to color in this figure legend, the reader is referred to the web version of this article.)

4.2. Custom outlet

The facts learned in section 4.1 can be seized to design improved μPGGs. On the one hand, the concentration profiles along linear cut lines such as the ones shown in Fig. 4a, are formed by streamlines of different lengths, i.e. shorter in the middle and longer in the extremes. As a consequence, the original gradient is slightly distorted. On the other hand, high α values slow down the solute dilution produced by transverse dispersion. Considering these issues, a new device can be thought in which the outlets are placed along an ellipse defined such that all streamlines have the same length. A diffuser with $\alpha = 90^{\circ}$ can be used to cool-down the concentration profile in a short distance, and simultaneously, to amplify the concentration gradient, making it more practical to handle. Furthermore, the outlets could be *continuous*, i.e. the border of the diffuser, or *discrete*, if different outlet arms are allowed after the diffuser. The complete μPGG was designed and modeled (Fig. 5). In particular, it is interesting to note that the concentration profiles obtained along different ellipses match perfectly, proving that the concentration profile can be effectively cooled-down (Fig. 5b).

Additionally, the distortion caused by streamlines of different lengths, could be exploited to customize the concentration profile in the outlets. For example, in Fig. 4, the bilinear cut line that results in a linear-like gradient could be used as an outlet pattern, where discrete outlets can be also included. The afore described μPGG was designed and modeled and its operation is condensed in Fig. 6. It is worth noting that a conventional microchannel gradient generators with radially distributed outlets has been reported [23].

Please cite this article in press as: F. Schaumburg, et al., Design keys for paper-based concentration gradient generators, J. Chromatogr. A (2018), https://doi.org/10.1016/j.chroma.2018.05.040

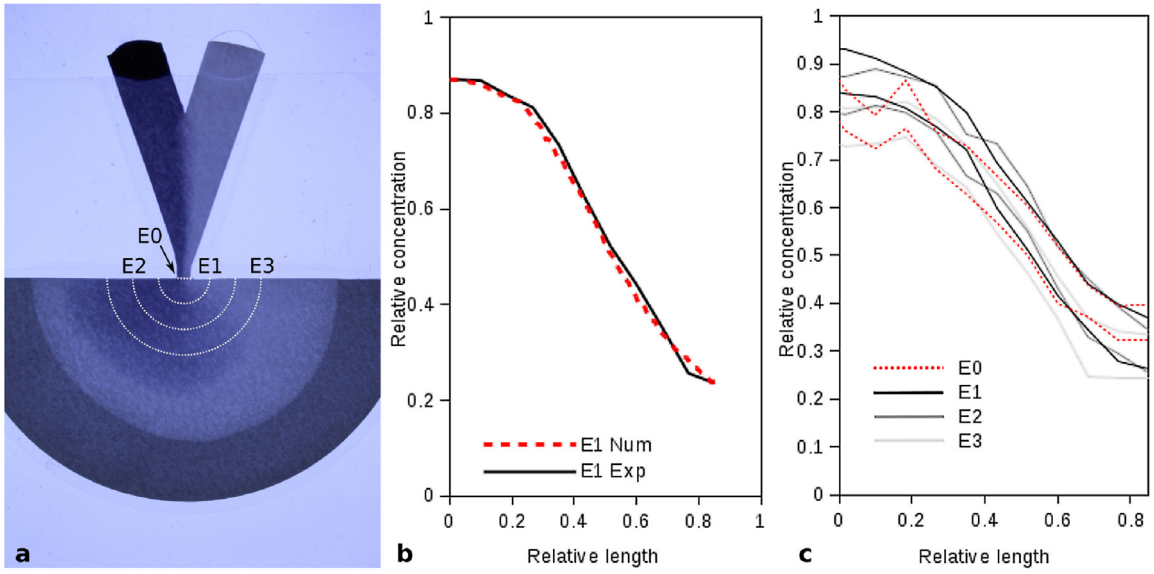

Fig. 7. Ellipsoidal outlet gradient generator: experimental control. (a) Picture of the real device; the outer fluid front is the prior wetting with pure water, the second front denotes the dye distribution after transverse dispersion in the flow domain. (b) Experimental concentration distribution along ellipse 1 (*E1* shown in 7a),where the dashed line is the numerical prediction for the same system. (c) Experimental concentration profiles obtained at *E0* and along the concentric ellipses shown in Fig. 7a). Such profiles are represented by uncertainty bands ($\pm 1SD$).

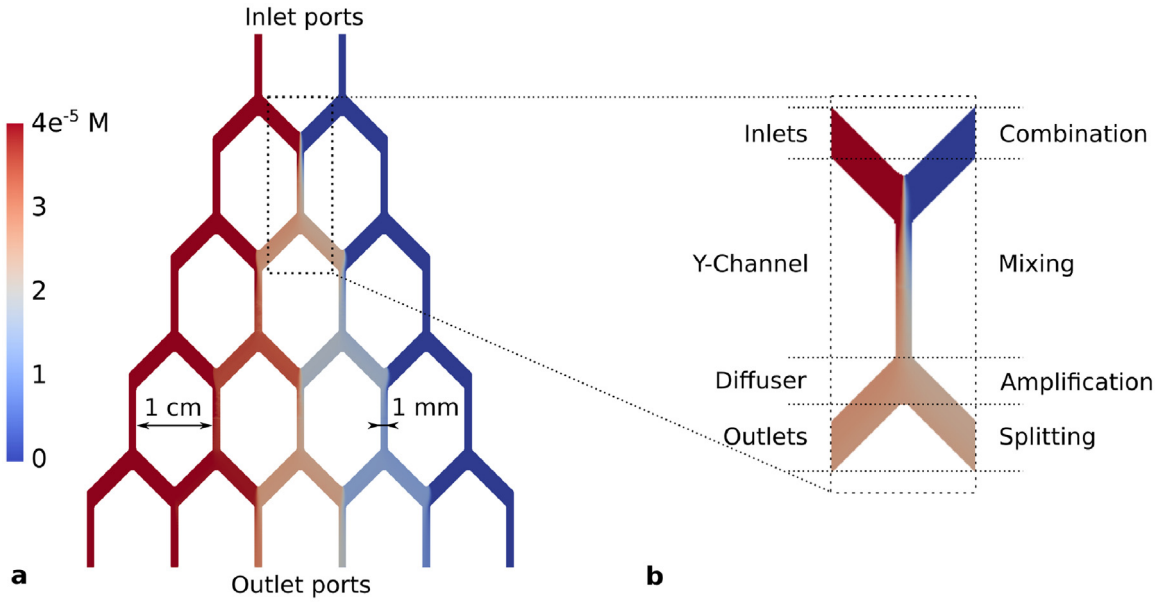

Fig. 8. In-plane tree format gradient generator. (a) Device dimensions and ports are depicted together with concentration distribution obtained numerically. (b) The elements forming the elementary structure and the operations performed in each element.

However, such a design cannot be obtained with the current μPADs manufacturing technology (the geometrical resolution available is not enough), whereas the design illustrated in Fig. 6 is suitable to be manufactured out of paper.

4.3. Physical prototype

In order to prove that the proposed numerical prototypes can be implemented in practice, as well as to verify the accuracy of the numerical predictions, physical prototypes were fabricated by craft-cutting. Whatman grade 1 filter paper was used as the material substrate, laminated with 150 μm thick film pouches to avoid evaporation. A 2%(v/v) water solution of a black hydro-soluble dye was used as the working sample. Absorbance of the transmitted light was optically measured to estimate local concentration. Further details on the experimental setup can be found in Ref. [19]. The dye concentration distribution obtained in a typical experiment is shown in Fig. 7a. Fig. 7b shows a comparison between numerical and experimental relative concentration profiles, which were taken along the normalized arc length of the ellipse *E1* indicated in Fig. 7a. Numerical data was normalized with the initial concentration C_0 while experimental data was normalized by subtracting the background (i.e. device image prior dye release). Then 13 equidistant points were taken along the *E1* ellipse, where a 50 pixel square region was centered to calculate the average intensity and the standard deviation (*SD*). The experimental profile was slightly shifted in the horizontal axis to align the mean value with the device symmetry axis. Finally min–max normalization was performed. The image

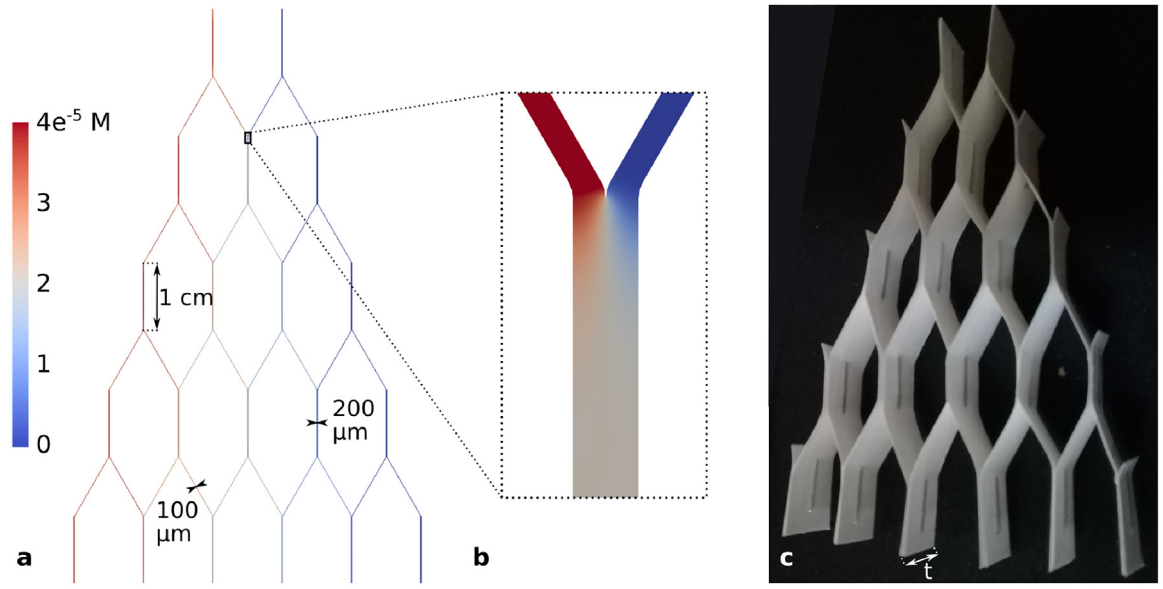

Fig. 9. Out-of-plane tree format gradient generator. (a) Device dimensions and concentration distribution obtained numerically. (b) The effective mixing in every branch occurs in the first millimeter. (c) Photograph of a device made out of office paper, just for the purposes of illustration.

processing was performed by using the ImageJ software [38]. In Fig. 7b, the average value is indicated in black. It can be seen that the agreement between experimental and numerical data is remarkable. Further, in Fig. 7c, experimental concentration profiles along *E0* to *E3* ellipses are superposed. In this case, concentration fields along *E0* to *E3* are indicated as bands, where the width of such bands is the estimated uncertainty expressed as $\pm 1SD$. This figure shows how the *DR* is maintained downstream in the diffuser, precisely as predicted by numerical simulations.

5. The tree format

5.1. Optimizing the branches shape

On the base of the knowledge gained in the previous examples, here we attempt to find a more efficient design for µPGGs with tree-like networks [11]. In this format, initial fluid streams (normally two, but also three can be used) are systematically split, mixed, and recombined throughout an increasing number of branches along a pyramidal network [25]. In the channels where mixing takes place, the elementary operation is the one studied in Section 3. Accordingly, the appropriate geometry to be used for branching is a Y-shaped juncture having a common channel with small *w* to reach mixing at short *l*, and then a symmetric expansion with splitting to connect neighbor branches. This operation unit must be repeated downstream up to reaching the desired branching level. The design proposed is shown in Fig. 8, which is based on a trade-off between the practical rules developed in the previous sections and the current technical capabilities of µPAD manufacturing techniques for an in-plane device, by using a single paper sheet.

5.2. Improving device throughput

The relatively small flow rate attainable in µPGGs may be a drawback for some applications like drug screening, where the throughput of the device is a primary requisite. The flow rate in each branch (hence in the whole device) is proportional to the paper thickness *h*, which is normally fixed by manufacturers. With these constraints, an attractive strategy is to design out-of-plane branching; for example, by using paper sheets in vertical position, including tie contact between sheets to form (double sheet) mixing channels. The gain in this configuration is twofold: (i) the dispersion width to be attained by the solute is just *h*, so that the mixing distance will be very short, and (ii) the depth of the channels *t* can be made as large as possible, in order to obtain higher flow rates. The design proposed is shown in Fig. 9.

The top view of the branching (Fig. 9a) is reminiscent of gradient generators made of threads in the form of fish-nets, where mixing is efficiently achieved in knots [39]. In such device, the low throughput is a concern as well, thus improving the flow rate by an external driving force was proposed [40]. In our paper-based design, mixing is effective due to the small transverse distance to be covered by dispersing species (which can be seen in Fig. 9b), and the improved throughput is equivalent to parallelizing the system by arranging a pile of networks. In fact, the flow rate in the proposed device is $20\,\mu L\,s^{-1}$ with $t = 5$ mm, or $40\,\mu L s^{-1}$ if $t = 1$ cm, that is 10 and 20 times bigger than the in-plane paper device in section 5.1. Fig. 9c illustrates the proposed 3D network structure.

6. Concluding remarks

The essential role played by mechanical dispersion on the analyte transport in µPADs makes necessary the introduction of novel strategies to design analytical operations, particularly for µPGGs. Some relevant concluding remarks are outlined as follows: first, it was shown in Section 3 that decreasing the width of the common channel reduces the final length of the device, increases the overall flow rate, and decreases the assay time (see also Ref. [19]). Second, a trade-off between *DR* and linearity was found in the gradient (refer to Fig. 2). Even though these conclusions also apply to conventional microchannels, they are particularly important in paper-based devices, as mechanical dispersion greatly emphasizes transverse solute dispersion. Third, a geometrical configuration that *cools-down* the effect of mechanical dispersion was found, which allows one to maintain a given concentration profile along the flow path. It consists in expanding the original channel with an angle α, in the form of a diffuser, which is easy to fabricate and manipulate. Fourth, these predictions were experimentally proved in devices made on Whatman 1 filter paper (see Fig. 7). Fifth, the concentration profile in the outlets can be adjusted to different functions in the range $[C_{MAX}, C_{MIN}]$, which is achieved by choosing

Please cite this article in press as: F. Schaumburg, et al., Design keys for paper-based concentration gradient generators, J. Chromatogr. A (2018), https://doi.org/10.1016/j.chroma.2018.05.040

the proper cut line in the diffuser and cutting the paper accordingly (see Fig. 4). Sixth, paper naturally enables the formation of continuous gradients, but also the possibility of delivering discrete concentration values by splitting the outlet into the desired number of fractions. It should be taken into account that these gradient generators are designed as a component to be integrated into more complex devices (see, for example, Refs. [11,12]). Seventh, in order to illustrate the utility of the above mentioned designing rules, the conventional tree-like format was redesigned to be implemented on paper, where the optimized Y-shaped mixer was included as the basic unit. Two novel pyramidal networks were prototyped: a 2D (in-plane paper, Fig. 8) and a 3D (vertical paper, Fig. 9). In particular, the last one is able to provide high throughputs. One may finally conclude that the suitable exploitation of mechanical dispersion in paper and similar porous substrates endows great potential to μPGGs.

Acknowledgements

This research was supported by CONICET (Grant PIP-0363), ANPCyT (Grant PICT-2016-0640), UTN (Grant PID ASUTNFE0004475), and UNL (Grant CAI+D-78-5012011010010-0), Argentina.

Appendix A. Supplementary data

Supplementary data associated with this article can be found, in the online version, at https://doi.org/10.1016/j.chroma.2018.05.040.

References

[1] W. Su, X. Gao, L. Jiang, J. Qin, Microfluidic platform towards point-of-care diagnostics in infectious diseases, J. Chromatogr. A 1377 (2015) 13–26.
[2] D.M. Cate, J.A. Adkins, J. Mettakoonpitak, C.S. Henry, Recent developments in paper-based microfluidic devices, Anal. Chem. 87 (2014) 19–41.
[3] M.M. Gong, D. Sinton, Turning the page: advancing paper-based microfluidics for broad diagnostic application, Chem. Rev. 117 (2017) 8447–8480.
[4] K. Yamada, H. Shibata, K. Suzuki, D. Citterio, Toward practical application of paper-based microfluidics for medical diagnostics: state-of-the-art and challenges, Lab. Chip 17 (2017) 1206–1249.
[5] R. Ota, K. Yamada, K. Suzuki, D. Citterio, Quantitative evaluation of analyte transport on microfluidic paper-based analytical devices (μpads), Analyst 143 (2018) 643–653.
[6] X. Wang, Z. Liu, Y. Pang, Concentration gradient generation methods based on microfluidic systems, RSC Adv. 7 (2017) 29966–29984.
[7] F. Deiss, A. Mazzeo, E. Hong, D.E. Ingber, R. Derda, G.M. Whitesides, Platform for high-throughput testing of the effect of soluble compounds on 3d cell cultures, Anal. Chem. 85 (2013) 8085–8094.
[8] D.I. Walsh III, M.L. Lalli, J.M. Kassas, A.R. Asthagiri, S.K. Murthy, Cell chemotaxis on paper for diagnostics, Anal. Chem. 87 (2015) 5505–5510.
[9] R.M. Kenney, M.W. Boyce, A.S. Truong, C.R. Bagnell, M.R. Lockett, Real-time imaging of cancer cell chemotaxis in paper-based scaffolds, Analyst 141 (2016) 661–668.
[10] D. Lantigua, Y.N. Kelly, B. Unal, G. Camci-Unal, Engineered paper-based cell culture platforms, Adv. Healthc. Mater. 6 (2017) 1700619.
[11] B. Hong, P. Xue, Y. Wu, J. Bao, Y.J. Chuah, Y. Kang, A concentration gradient generator on a paper-based microfluidic chip coupled with cell culture microarray for high-throughput drug screening, Biomed. Microdev. 18 (2016) 21.
[12] M. Mercuri, R. Gimenez, C. Berli, M. Bellino, Configurable 2D nano-flows in mesoporous films using paper patches, RSC Adv. 8 (2018) 6414–6418.
[13] I. Jang, G. Kim, S. Song, Mathematical model for mixing in a paper-based channel and applications to the generation of a concentration gradient, Int. J. Heat Mass Transf. 120 (2018) 830–837.
[14] J.L. Osborn, B. Lutz, E. Fu, P. Kauffman, D.Y. Stevens, P. Yager, Microfluidics without pumps: reinventing the t-sensor and h-filter in paper networks, Lab. Chip 10 (2010) 2659–2665.
[15] A.R. Rezk, A. Qi, J.R. Friend, W.H. Li, L.Y. Yeo, Uniform mixing in paper-based microfluidic systems using surface acoustic waves, Lab. Chip 12 (2012) 773–779.
[16] J. Bear, Dynamics of Fluids in Porous Media, American Elsevier Publishing Company, 1972.
[17] B.P. van Milligen, P.D. Bons, Analytical model for tracer dispersion in porous media, Phys. Rev. E 85 (2012) 011306.
[18] A. Daneyko, D. Hlushkou, S. Khirevich, U. Tallarek, From random sphere packings to regular pillar arrays: analysis of transverse dispersion, J. Chromatogr. A 1257 (2012) 98–115.
[19] R. Urteaga, E. Elizalde, C.L. Berli, Transverse solute dispersion in paper-based microfluidics, Analyst 143 (2018) 2259–2266.
[20] J. Atencia, J. Morrow, L.E. Locascio, The microfluidic palette: a diffusive gradient generator with spatio-temporal control, Lab. Chip 9 (2009) 2707–2714.
[21] T. Frank, S. Tay, Flow-switching allows independently programmable, extremely stable, high-throughput diffusion-based gradients, Lab. Chip 13 (2013) 1273–1281.
[22] D. Kilinc, J. Schwab, S. Rampini, O.W. Ikpekha, A. Thampi, A. Blasiak, P. Li, R. Schwamborn, W. Kolch, D. Matallanas, G.U. Lee, A microfluidic dual gradient generator for conducting cell-based drug combination assays, Integr. Biol. 8 (2016) 39–49.
[23] M.A. Holden, S. Kumar, E.T. Castellana, A. Beskok, P.S. Cremer, Generating fixed concentration arrays in a microfluidic device, Sens. Actuators B 92 (2003) 199–207.
[24] H. Mao, P.S. Cremer, M.D. Manson, A sensitive, versatile microfluidic assay for bacterial chemotaxis, Proc. Natl. Acad. Sci. U. S. A. 100 (2003) 5449–5454.
[25] N.L. Jeon, S.K. Dertinger, D.T. Chiu, I.S. Choi, A.D. Stroock, G.M. Whitesides, Generation of solution and surface gradients using microfluidic systems, Langmuir 16 (2000) 8311–8316.
[26] B.G. Abdallah, S. Roy-Chowdhury, R. Fromme, P. Fromme, A. Ros, Protein crystallization in an actuated microfluidic nanowell device, Cryst. Growth Des. 16 (2016) 2074–2082.
[27] D. Irimia, D.A. Geba, M. Toner, Universal microfluidic gradient generator, Anal. Chem. 78 (2006) 3472–3477.
[28] K. Lee, C. Kim, B. Ahn, R. Panchapakesan, A.R. Full, L. Nordee, J.Y. Kang, K.W. Oh, Generalized serial dilution module for monotonic and arbitrary microfluidic gradient generators, Lab. Chip 9 (2009) 709–717.
[29] C.-Y. Chen, A.M. Wo, D.-S. Jong, A microfluidic concentration generator for dose-response assays on ion channel pharmacology, Lab. Chip 12 (2012) 794–801.
[30] S. Sugiura, K. Hattori, T. Kanamori, Microfluidic serial dilution cell-based assay for analyzing drug dose response over a wide concentration range, Anal. Chem. 82 (2010) 8278–8282.
[31] F. Schaumburg, P.A. Kler, C.L. Berli, Numerical prototyping of lateral flow biosensors, Sens. Actuators B – Chem. 259 (2018) 1099–1107.
[32] H. Gerke, M.V. Genuchten, A dual-porosity model for simulating the preferential movement of water and solutes in structured porous media, Water Resour. Res. 29 (1993) 305–319.
[33] S.P. Neuman, D.M. Tartakovsky, Perspective on theories of non-fickian transport in heterogeneous media, Adv. Water Resour. 32 (2009) 670–680.
[34] J. Crank, The Mathematics of Diffusion, Oxford University Press, 1979.
[35] E. Elizalde, R. Urteaga, C.L. Berli, Rational design of capillary-driven flows for paper-based microfluidics, Lab. Chip 15 (2015) 2173–2180.
[36] R. Masoodi, K.M. Pillai, Darcy's law-based model for wicking in paper-like swelling porous media, AIChE J. 56 (2010) 2257–2267.
[37] P.A. Kler, L.D. Dalcin, R.R. Paz, T.E. Tezduyar, Supg and discontinuity-capturing methods for coupled fluid mechanics and electrochemical transport problems, Comput. Mech. 51 (2013) 171–185.
[38] C.T. Rueden, J. Schindelin, M.C. Hiner, B.E. DeZonia, A.E. Walter, E.T. Arena, K.W. Eliceiri, Imagej2: Imagej for the next generation of scientific image data, BMC Bioinform. 18 (1) (2017) 529.
[39] R. Safavieh, G.Z. Zhou, D. Juncker, Microfluidics made of yarns and knots: from fundamental properties to simple networks and operations, Lab. Chip 11 (2011) 2618–2624.
[40] S. Ramesan, A.R. Rezk, K.W. Cheng, P.P. Chan, L.Y. Yeo, Acoustically-driven thread-based tuneable gradient generators, Lab. Chip 16 (2016) 2820–2828.

Please cite this article in press as: F. Schaumburg, et al., Design keys for paper-based concentration gradient generators, J. Chromatogr. A (2018), https://doi.org/10.1016/j.chroma.2018.05.040